Conversion of a Porin-like Peptide Channel into a Gramicidin-like Channel by Glycine to D-alanine Substitutions

Jyothi Thundimadathil, Roger W. Roeske, and Lili Guo
Department of Biochemistry and Molecular Biology, Indiana University School of Medicine, Indianapolis, Indiana 46202

ABSTRACT The β-barrel and β-helix formation, as in porins and gramicidin, respectively, represent two distinct mechanisms for ion channel formation by β-sheet proteins in membranes. The design of β-barrel proteins is difficult due to incomplete understanding of the basic principles of folding. The design of gramicidin-like β-helix relies on an alternating pattern of L- and D-amino acid sequences. Recently we noticed that a short β-sheet peptide $(xSxG)_6$, can form porin-like channels via self-association in membranes. Here, we proposed that glycine to D-alanine substitutions of the *N*-formyl-$(xSxG)_6$ would transform the porin-like channel into a gramicidin-like β^{12}-helical channel. The requirement of an *N*-formyl group for channel activity, impermeability to cations with a diameter >4 Å, high monovalent cation selectivity, and the absence of either voltage gating or subconductance states upon D-alanine substitution support the idea of a gramicidin-like channel. Moreover, the circular dichroism spectrum in membranes is different, indicating a change in regular β-sheet backbone structure. The conversion of a complex porin-like channel into a gramicidin-like channel provides a link between two different mechanisms of β-sheet channel formation in membranes and emphasizes the importance of glycine and D-amino acid residues in protein folding and function and in the engineering of ion channels.

INTRODUCTION

Design of peptides mimicking the complex functional properties (voltage gating, ion selectivity, molecular transport, etc.) of natural ion channels is an important goal in membrane protein engineering due to the possibilities of developing novel macromolecular devices and therapeutics. However, the rational design of such systems is difficult as the fundamental principles of membrane binding, membrane insertion, self-assembly, folding, and channel gating of proteins are not clearly understood. For example, a better understanding of the basic principles of folding and pore formation by β-sheet peptides in membranes (1–3) will have far-reaching implications in developing therapeutics for different protein conformational diseases and also in the de novo design of β-barrel proteins (4–8). In this context, recently we observed that a short β- sheet peptide, $(xSxG)_6$, (VSLGLSIGFSVGVSIGWSFGRSRG) forms voltage-gated, high-conductance multichannels closely resembling β-barrel porins in lipid bilayers (9). A detailed study of the aggregation, channel activity, and peptide-lipid interactions indicated the insertion of the peptide as oligomers into the lipid bilayer followed by rearrangement into a complex β- barrel-like pore structure comprising several individual β-sheets or smaller β-sheet aggregates (10). A dyad repeat sequence and the presence of glycine, serine, and hydrophobic residues similar to that found in β-barrel proteins are considered as the driving force for porin-like channel formation by this peptide (10).

The unprecedented observation of the porin-like activity by a short β-sheet peptide with a repeating sequence pattern could provide a useful platform for elucidating the effect of specific amino acid residues on folding and functional properties of β-sheet peptides in membranes and structural engineering through amino acid replacements. In this work, we substituted four out of six glycine residues of $(xSxG)_6$ with D-alanines (VSLGLSI*A*FSV*A*VSI*A*WSF*A*RSRG, where *A* is D-alanine; abbreviated as $(xSxA/G)_6$) to examine its effect on conformational and ion channel properties. Peptides having a regularly repeating pattern of L and D amino acids are known to adopt unique structures, especially in membranes (e.g., the single stranded head-to-head β^6-helical dimer structure of gramicidin A (gA)) (11–15). Here, we hypothesized that substitutions of small, flexible glycine residues with D-alanines in $(xSxG)_6$ would lead to a dramatic change in its structural and functional properties. Thus the *N*-formyl analog of $(xSxA/G)_6$ is likely to form a β^{12}-helical dimeric structure similar to that of gA as proposed by Kennedy et al. for a *N*-formyl-$(LLLD)_6$ sequence (16,17). In a β^{12}-helical model, it is possible to have polar side chains (e.g., serine) inside the helical pore and hydrophobic side chains pointing outside, thereby satisfying the condition for an ideal ion channel inside a lipid bilayer (Fig. 1).

MATERIALS AND METHODS

Reagents for peptide synthesis, viz., 2-(1H-benzotriazol-1-yl)1,1,3,3-tetramethyluronium hexafluorophosphate (HBTU), 1-hydroxybenzotriazole (HOBT), *N*,*N*-diisopropylethylamine (DIEA), *N*-methylpyrrolidone (NMP), dichloromethane, piperidine, trifluoroacetic acid (TFA), and Kaiser reagent were of peptide synthesis grade purchased from Applied Biosystems (Foster City, CA). Gly-Wang resin and Fmoc-protected amino acids were available from Advanced Chem Tech (Louisville, KY). All other solvents used were

Submitted August 16, 2005, and accepted for publication October 19, 2005.

Address reprint requests to Lili Guo, Dept. of Biochemistry and Molecular Biology, Indiana University School of Medicine, 635 Barnhill Dr., Indianapolis, IN 46202. Tel.: 317-274-7507; Fax: 317-274-4686; E-mail: lguo@iupui.edu.

0006-3495/06/02/947/09 $2.00

doi: 10.1529/biophysj.105.072751

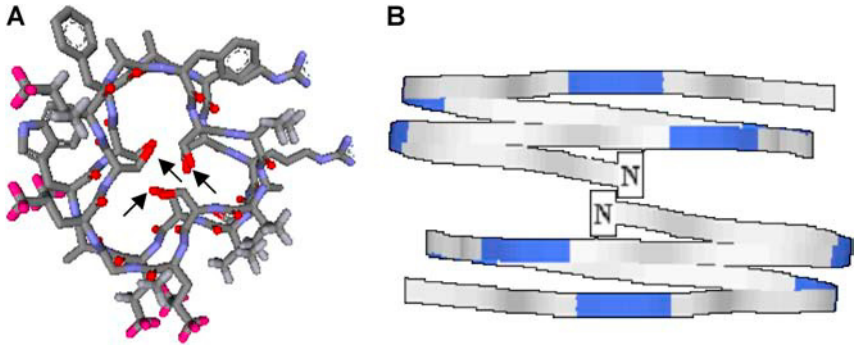

FIGURE 1 (*A*) An axial view of a β^{12}-helical model proposed for f-(xSx*A*/G)$_6$ peptide (formyl-VSLGLSI*A*FSV*A*VSI*A*WSF*A*RSRG, where *A* is D-alanine) showing hydrophilic serine hydroxyls located inside the pore (marked with *arrows*) and all hydrophobic side chains pointing outside. One turn of the β^{12}-helix comprises 12 amino acid residues, and hence a total of 24 amino acids makes two β-helical turns. (*B*) A β^{12}-helical dimer formed by the association of two β^{12} units through *N*-formyl groups as in gA.

of HPLC grade purchased from Fisher Scientific (Fair Lawn, NJ). Diphytanoylphosphatidylcholine (DPhPC) and dimyristoylphosphatidylcholine (DMPC) were purchased from Avanti Polar Lipids (Alabaster, AL).

Peptide synthesis

The (xSxG)$_6$ and (xSx*A*/G)$_6$ peptides were synthesized manually using standard solid phase Fmoc chemistry as explained earlier (9,10). The *N*-formylation was carried out with p-nitrophenyl formate in *N*-methyl pyrrolidone. The *N*-formyl and desformyl analogs of the above peptides are indicated as f- and df-, respectively. The peptides were purified by reverse phase HPLC (a Varian Prostar 210 system fitted with a Prostar 320 ultraviolet/visible detector) on a C_4 column (Vydac; 5 μm particle size, 10 mm i.d., and 250 mm length). A methanol-water gradient (solution A: 100% H_2O, 0.1% TFA; solution B: 100% CH_3OH, 0.09% TFA; Program: B—70% (0 min)-70% (20 min)-90% (39 min)-90% (60 min)-95% (61 min)-100% (85 min)) was used for elution. The collected methanol-water fractions were lyophilized after removing methanol by rotary evaporation. The peptides were characterized by analytical HPLC and molecular weight analysis using a MALDI-TOF (matrix assisted laser desorption-time of flight) mass spectrometer (Micromass, Manchester, UK). The peptide purity was >95%.

Planar lipid bilayer studies

Planar lipid bilayers were formed by applying DPhPC solution (15 mg/mL in *n*-decane) over a 200 μm diameter aperture in the wall of a Delrin cup (18). Typically, ~3 μL of a methanolic solution of f-(xSx*A*/G)$_6$ peptide (0.05 mg/mL) was added to both sides of the preformed bilayer membranes containing 100–1000 mM CsCl solution (unbuffered) to a final concentration of $\sim 10^{-8}$ M. A custom current/voltage conversion amplifier was used to optimize single-channel recording. The Ag/AgCl electrodes were connected to the *cis* and *trans* chambers through 1 M KCl-agar bridges (the side which was connected to the signal ground of the amplifier is defined as *trans*, and the opposite side to which lipid solution was smeared is defined as *cis*). Transmembrane currents through voltage-clamped bilayers were low-pass filtered at 1 kHz using an 8-pole Bessel filter (model BC-525C, Warner Instrument Co., Hamden, CA) followed by digitization at 0.5 kHz with a 16 bit data acquisition system (Digidata 1320 A, Axon Instruments, Foster City, CA). The data were acquired and analyzed using a computer and Clampex 8.2 software (Axon Instruments). Curve fits were done using the Marquardt least-squares algorithm.

Peptide-unilamellar lipid vesicles

The peptide-liposomes were prepared by a modified method of Wallace and Blout (19); ~0.5 mg of peptide and 5 mg of DMPC (peptide/lipid molar ratio 1:36) were codissolved in 2 mL trifluoroethanol followed by removal of the solvent to get a peptide-lipid film. The lipid film was hydrated with 500 μL of D_2O (or H_2O) and incubated at 40°C for 2 h followed by sonication for 5 min using a Branson sonifier 450 (output control 4, duty cycle 30%, 35 watts) fitted with a contact tip accessory. Samples were centrifuged at 14,000 rpm for 10 min at room temperature. After these treatments a clear solution was obtained. Liposomes without peptides were also prepared as a control.

Circular dichroism spectroscopy

Circular dichroism (CD) measurements were carried out at 20°C on a JASCO (Easton, MD) J-720 spectrometer. The ellipticity was calibrated with (+)-10-camphorsulfonic acid. Each spectrum was an average of 6–30 scans using quartz cells having path lengths of 0.01 or 0.05 cm. Spectra were recorded in the range 260–180 nm at a speed of 50 nm/min with a resolution of 0.2 nm and are presented on a per amide basis (deg cm^2 decimol^{-1}). The mean residue molar ellipticity $[\Theta]_{MRW}$ was calculated using the formula, $[\Theta]_{MRW} = \Theta/10 \times Cr \times l$, where *MRW* is the mean residue weight (molecular weight/number of residues) of the peptide, Cr is the mean residue molar concentration ($Cr = n \times Cp$, where n is the number of peptide bonds and Cp is the molar concentration in mol/liter), l is the path length in cm, and Θ is the ellipticity in mdeg.

IR spectroscopy

Attenuated total reflectance-Fourier transform infrared spectroscopy (ATR-FTIR) spectra were recorded on a Perkin Elmer 2000 spectrometer. Typically, aliquots of 50 μL peptide-liposome samples were loaded onto a ZnSe internal reflection element (IRE) and a hydrated thin film was formed by using a stream of nitrogen gas. The IRE was then placed in an ATR accessory, and FTIR spectra were collected. The background spectrum was collected using the same IRE before the sample measurements. Fourier deconvoluted and second derivative spectra were obtained using Grams analyst 2000 software. Resulting spectra were smoothed by the 7 point Savitsky-Golay function. Band fittings of the deconvoluted spectra were done using a Gaussian function, and starting band parameters were taken from deconvoluted spectra. The initial line widths were set to 12 cm^{-1} and allowed to vary freely. The relative areas of the components were expressed as a percentage of the area of each fitted region, which was equivalent to an area normalization of the amide bands.

RESULTS

Effect of Gly to D-Ala substitutions on channel activity

The single-channel conductance of f-(xSx*A*/G)$_6$ was examined in a symmetrical aqueous solution of CsCl (1 M, unbuffered) under voltage clamp conditions at 25°C. Addition

of ~3 μL of a methanolic solution (0.05 mg/mL) of the peptide on both sides of the bilayer resulted in rapid transitions between the open and closed states and stable current levels typical of single channels. Similar current transitions were difficult to observe when the peptide was added only on one side of the bilayer. Typical channel traces obtained at different applied potentials are shown in Fig. 2 *A*. A linear current-voltage relationship was obtained under symmetrical ionic conditions (Fig. 2 *B*). The single-channel conductance as determined from the slope of the I/V curve was 49.6 pS with a 1 M CsCl (unbuffered) solution. The desformyl analog of $(xSxA/G)_6$ failed to show any ion channel activity, whereas both the formyl and desformyl analogs of $(xSxG)_6$ peptide formed high conductance channels under similar experimental conditions (9). The channel trace of f-$(xSxG)_6$ obtained at an applied potential of 10 mV after the addition of 3 μL of a methanolic solution (0.05 mg/mL) of the peptide on one side of the bilayer (channels appeared immediately after the addition of the peptide on the *cis* side of the bilayer) is shown for comparison (Fig. 2 *C*). The single-channel conductance of f-$(xSxG)_6$ (1370 pS) was ~28 times the conductance of f-$(xSxA/G)_6$ channels (compare the scale in Fig. 2, *A* and *C*). The f-$(xSxG)_6$ channel was in the high conductance open state most of the time, and complete closures were rarely seen at low applied potentials. Moreover, several fast flickering type events along with short-lived subconductance states were seen in f-$(xSxG)_6$ channels. On the contrary, the most important characteristics of f-$(xSxA/G)_6$ channel were the absence of multichannels or subconductance states and the occurrence of complete closing events at different applied potentials.

All-point histograms generated from typical channel traces are shown in Fig. 3. Two sharp peaks clearly demonstrating a closed and an open state can be found in the case of the f-$(xSxA/G)_6$ channel (Fig. 3, *A* and *B*), whereas in the f-$(xSxG)_6$ channel relatively broader peaks (extending over ~4 pA in the *x* axis) representative of mainly two levels, a low conductance state and a high conductance state, were seen (Fig. 3 *C*). The ion channel data were further analyzed by generating open times distributions corresponding to the open conductance state using dwell-time histograms. The binned data were fitted exponentially using the Marquardt least-squares algorithm. The open time events in f-$(xSxA/G)_6$ channel events could be best fitted with a single time constant (Fig. 3, *D* and *E*). However, in f-$(xSxG)_6$ channels the openings to the large conductance state are best characterized with two time constants (τ_1 and τ_2) indicating the complex nature of the channel (Fig. 3 *F*).

Voltage dependence of channels

The voltage dependences of both the f-$(xSxA/G)_6$ and f-$(xSxG)_6$ channels were analyzed by estimating the proportion of the open state component at different applied potentials by Gaussian fitting of the all-point histograms. The fractional contributions of the open state component to the total area under the curve at different applied potentials are shown in Fig. 4. In the case of f-$(xSxA/G)_6$, the fraction of open channel events remained almost the same at different voltages, suggesting little voltage dependence on channel activity. It can be seen that ~40% of the total events represent the open state of the channel. The proportion of the high conductance channel component in f-$(xSxG)_6$ channel was maximum (>80%) at low applied potentials (<±40 mV) and a sharp decrease in the high conductance open channel events was observed at higher potentials, showing

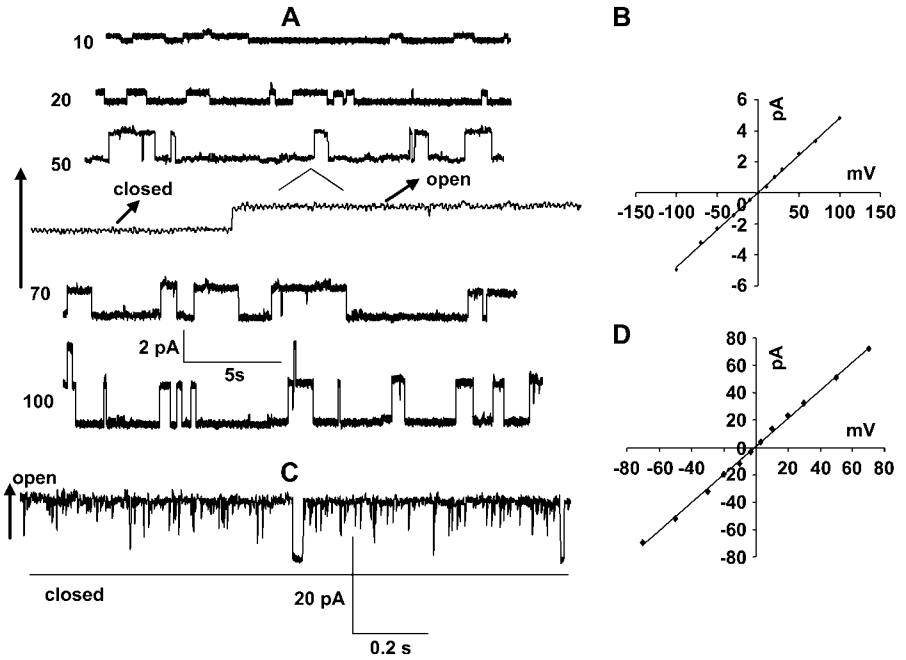

FIGURE 2 (*A*) Single channels (49.6 pS) formed by f-$(xSxA/G)_6$ (3 μL of 0.05 mg/mL methanolic solution added on both sides of the bilayer) at different applied potentials (10–100 mV) in 1 M CsCl (unbuffered) solution under symmetrical conditions. The channel trace at 50 mV is also shown in an expanded timescale. The df-$(xSxA/G)_6$ did not form channels. (*B*) The current-voltage (I/V) relationship of f-$(xSxA/G)_6$ channels under symmetrical conditions. (*C*) A typical channel trace obtained for f-$(xSxG)_6$ at an applied potential of 10 mV in 1 M CsCl (unbuffered) after the addition of 3 μL of 0.05 mg/ml methanolic solution of the peptide to *cis* side, showing high conductance opening (1370 pS) and multiple short-lived closers to subconductance states. Channels open in the direction of arrows and dotted lines represent a zero current level. (*D*) I/V relationship of f-$(xSxG)_6$ channels under symmetrical conditions.

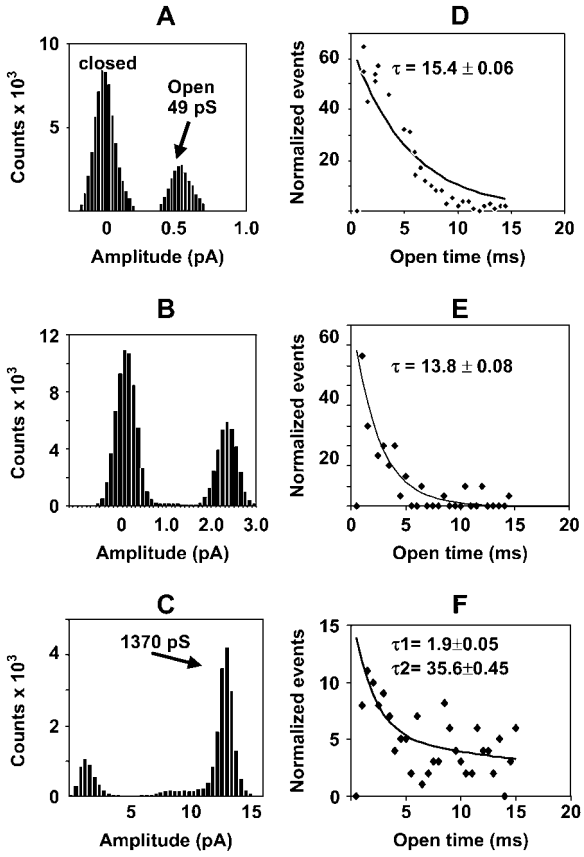

FIGURE 3 (*A* and *B*) All-point histograms generated from typical channel traces of f-(xSx*A*/G)$_6$ at 10 and 50 mV, respectively, showing distinct closed and open states of the channel. The mean single-channel conductance of f-(xSx*A*/G)$_6$ channel is ~49 pS. (*C*) All-point histogram generated from the channel trace of f-(xSxG)$_6$ shown in Fig. 2 showing low conductance and high conductance states along with some subconductance states. The mean single-channel conductance of the f-(xSxG)$_6$ channel is found to be 1370 pS. (*D–F*) The open time distributions generated for the open state of the channels on the left using dwell-time histograms of the data. The binned data (bin width = 0.5 ms) were fitted exponentially using Marquardt least-squares algorithm. The open channel events of the f-(xSx*A*/G)$_6$ channel are best characterized with a single time constant, whereas openings to the large conductance state of f-(xSxG)$_6$ are best characterized with two time constants (τ1 and τ2).

a voltage-dependent behavior. A two state voltage gating of f-(xSxG)$_6$ channels with a tendency to close both at positive and negative potentials at applied potentials >40 mV has already been reported (9).

Charge selectivity of channels

The charge selectivity of the f-(xSx*A*/G)$_6$ channel was determined from zero-current potentials of I/V curves under asymmetric conditions. K^+ and Cl^- ions usually have about the same mobility in aqueous solutions, and hence zero current potential in the presence of KCl salt gradients (500:100 mM) was measured. Under these conditions a zero current potential of −29.6 mV was obtained corresponding to a permeability ratio (pK^+/pCl^-, calculated using the Goldman-Hodgkin-Katz (GHK) equation) of 6.9, indicating that the f-(xSx*A*/G)$_6$ channel is cation selective (Fig. 5). However, the f-(xSxG)$_6$ channel showed little preference to cations over anions as indicated by a zero current potential of −9 mV and corresponding permeability ratio (pK^+/pCl^-) of 2.1 (9).

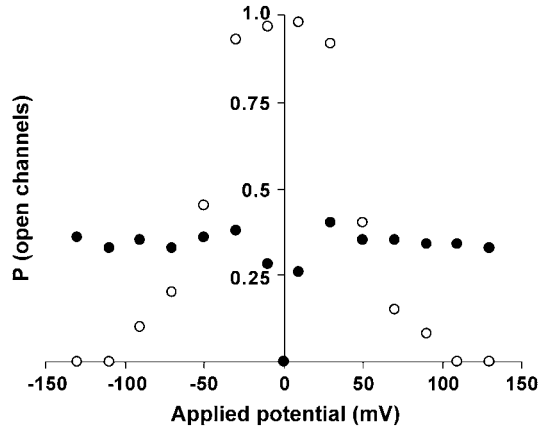

FIGURE 4 Voltage dependence of channels. The proportion of open state component of f-(xSx*A*/G)$_6$ (●) and f-(xSxG)$_6$ peptide (○) channels at different applied potentials obtained by Gaussian fitting of the all-point-histograms of channel data. In the case of f-(xSx*A*/G)$_6$, the fraction of open channel events remained almost the same at different voltages, suggesting little voltage dependence on channel activity. The proportion of the high conductance channel component in f-(xSxG)$_6$ channels is maximum (>80%) at low applied potentials (<±40 mV), and a sharp decrease in high conductance open channel events can be seen at higher potentials, showing a voltage-dependent behavior.

Pore diameter of peptide channels

We observed earlier that the f-(xSxG)$_6$ channel transports a variety of ions such as Cs^+, K^+, Na^+, Li^+, Ca^{2+}, NH_4^+, NMe_4^+, NEt_4^+, NEt_3Bz^+, and glucosammonium, suggesting a pore diameter >10.5 Å corresponding to the diameter of the largest permeating cation (NEt_3Bz^+) obtained from Corey, Pauling, and Koltun (space-filling) models (9). A comparative

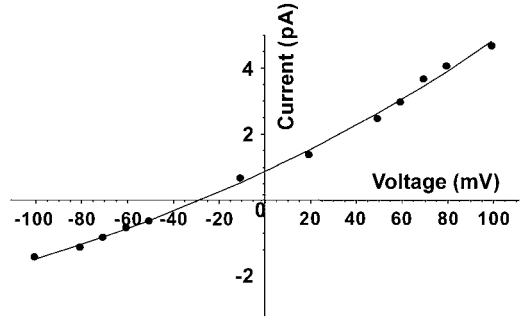

FIGURE 5 Current-voltage (I/V) relationship of the f-(xSx*A*/G)$_6$ channel under asymmetrical conditions (*cis*/*trans*, 500/100 mM KCl). The solid line was drawn according to the least-square procedure using the Marquardt-Levenberg algorithm. A zero current potential of −29.6 mV and permeability ratio $pK^+/pCl^- = 6.9$ was obtained according to the GHK equation, indicating a cation-selective channel.

account of single-channel conductance of f-$(xSxG)_6$ and f-$(xSxA/G)_6$ channels in the presence of different electrolytes under similar experimental conditions are given in Table 1. Among the organic cations tested, only the ammonium ion (4 Å) was permeable in the case of the f-$(xSxA/G)_6$ channel, and measurable channel activity was not observed in the presence of electrolytes containing larger cations such as NMe_4^+, NEt_4^+, glucosammonium, and NEt_3Bz^+ with a diameter of 6, 9, 10, and 10.5 Å, respectively, indicating a relatively smaller pore compared to the f-$(xSxG)_6$ channel. Based on these observations, we believe that the diameter of the narrowest portion of the f-$(xSxA/G)_6$ channel should be ~4 Å similar to gramicidin channel. The selectivity sequence in terms of conductances or conductance ratios of the f-$(xSxA/G)_6$ channel for monovalent cations followed the order Cs > K> Na >Li. The conductance in CsCl is ~3 times that in LiCl solution, which suggests that the channel favors the passage of Cs over Li cation. Although the radius of bare Cs ion (1.69 Å) is much larger than that of lithium (0.6 Å), the inner hydration shell of the former is small and is easily dehydrated. Therefore the process of cation passage through the peptide channel might be controlled predominantly by dehydration energies (20). Moreover, the overall ion selectivity of the channel could be influenced by other factors like the effective size of the pore and the electrostatic interaction between the ions and the pore interior.

Dependence of channel conductance on peptide concentration

To examine whether the channel is formed by the association of two or more peptide molecules, the relationship between f-$(xSxA/G)_6$ concentration and membrane conductance was determined by measuring the conductance (Λ) at various peptide concentrations (C). The data were plotted on a log-log scale (Fig. 6). From the obtained relationship log (Λ) = 1.7 log (C), the value of slope (1.7) gives an approximate estimate of the number of molecules per channel (21). This method would give only an approximate value of peptide units comprising the channel due to the difficulty in knowing the exact number of molecules moved into lipid bilayer at various peptide concentrations. Nevertheless, the value of 1.7 could be considered as a lower limit of peptide units required for channel formation.

TABLE 1 Mean single-channel conductances of peptide channels in different electrolytes*

	f-$(xSxG)_6$		f-$(xSxA/G)_6$	
Electrolyte Solution	$\Lambda^\dagger$	$\Lambda/\Lambda_0^\ddagger$	Λ	Λ/Λ_0
CsCl	1350 ± 40	1.02	49 ± 1.5	1.24
KCl	1320 ± 55	1.0	39.5 ± 1.8	1.0
CH_3COOK	1310 ± 43	0.99	37 ± 0.5	0.94
NaCl	1100 ± 52	0.83	30.8 ± 1.0	0.78
LiCl	800 ± 65	0.60	16.1 ± 0.5	0.41
NH_4Cl	1600 ± 35	1.21	28.5 ± 0.8	0.72
$CaCl_2$	1550 ± 32	1.14	–	–
NMe_4Cl	720 ± 18	0.54	–	–
NEt_4Cl	680 ± 24	0.51	–	–
$NEt_3BzCl^\S$	80 ± 8.5	–	–	–
$GluCl^\S$	130 ± 11	–	–	–

*1 M unbuffered solutions of the electrolytes used under symmetrical conditions and 3 μL of a methanolic solution of the peptide (0.05 mg/mL) was added close to the DPhPC lipid bilayers using a micropipette.

$^\dagger\Lambda$ is the mean single-channel conductance. Each conductance value is represented as mean ± SD from more than one experiment.

‡The conductance ratio, $\Lambda/\Lambda 0$, is the conductance in presence of each electrolyte relative to that in KCl solution.

§100 mM solutions of NEt_3BzCl and glucosamine hydrochloride (GluCl) were used.

CD spectra of f-$(xSxA/G)_6$ and f-$(xSxG)_6$ in membranes

Conformations of different peptides in a membrane-mimicking environment were examined using CD and infrared spectroscopy. CD spectra of f-$(xSxA/G)_6$, df-$(xSxA/G)_6$, and f-$(xSxG)_6$ incorporated in liposomes are shown in Fig. 7. Also a spectrum of f-$(xSxA/G)_6$ in methanol solution is given for comparison. Two distinct minima at 215.6 and 225.5 nm were observed in the spectrum of f-$(xSxA/G)_6$-incorporated liposomes along with two maxima around 200 nm. The df-$(xSxA/G)_6$-incorporated liposomes produced a slightly different spectrum with a broad band in the region 212–226 nm with a distinct minimum around 217.6 nm (maximum around 195 nm). The spectrum of f-$(xSxG)_6$-incorporated liposomes was characterized by a negative band around 220 nm and a positive band around 202 nm, indicating the folding of peptides into a β-structure in membranes (13,22). In methanol, the spectrum of f-$(xSxA/G)_6$ displayed a maximum around 198 nm and a minimum around 219 nm, suggesting predominantly a β-structure in solution.

IR spectra of f-$(xSxA/G)_6$ and df-$(xSxA/G)_6$-incorporated liposomes

Deuterium oxide (D_2O) was selected as the solvent during liposome preparation to avoid the interference from arginine

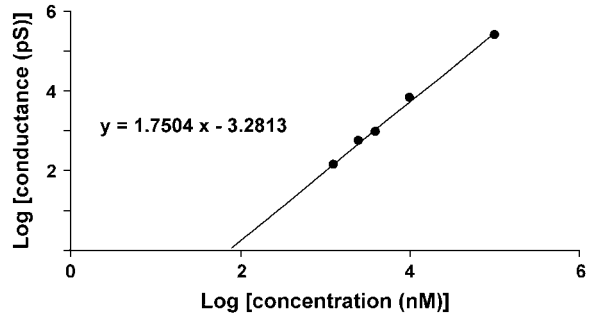

FIGURE 6 Membrane conductance as a function of f-$(xSxA/G)_6$ concentration. The slope of the linear equation indicates that the peptide-induced conductance is approximately the second order function of its concentration in the aqueous phase surrounding the membrane. Each data point on the graph represents the average value obtained from five measurements. Experimental conditions same as in Fig. 2.

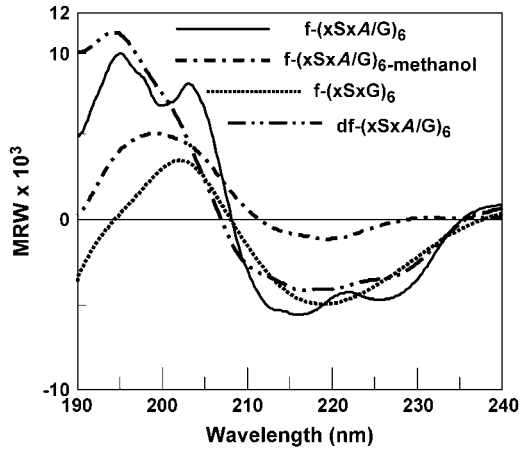

FIGURE 7 CD spectra of peptide-incorporated liposomes (DMPC/peptide = 1:36). The spectrum of f-(xSxG)$_6$ shows a characteristic β-sheet backbone structure, whereas the spectrum of f-(xSx*A*/G)$_6$ is different in having an additional band at 226 nm. The spectrum of f-(xSx*A*/G)$_6$ in methanol resembles that of a β-sheet protein.

side-chain absorption in the amide 1 region (23). The arginine absorptions near 1635 cm^{-1} and 1673 cm^{-1} usually exhibit large shifts of -50 and -70 cm^{-1}, respectively, upon hydrogen/deuterium exchange (23). This was confirmed by a comparative analysis of the secondary derivative spectra in water and D_2O solutions (data not shown). The main feature of the amide 1 region of the spectra of f-(xSx*A*/G)$_6$- and df-(xSx*A*/G)$_6$-incorporated liposome samples was the occurrence of a strong band around 1627 cm^{-1} and another in the high frequency region around 1690 cm^{-1} (Fig. 8). The spectral bands could be resolved into at least five individual absorptions that are centered around 1692, 1684, 1669, 1652, and 1627 cm^{-1} through deconvolution (Table 2). The occurrence of a 1627 cm^{-1} band with a high percentage relative area (~60%, see Table 2) suggests predominantly a β-conformation in membranes (24). The high

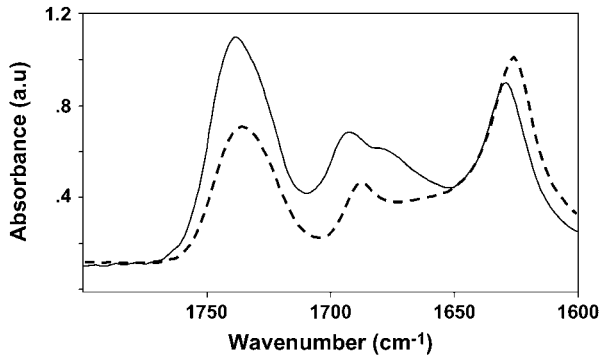

FIGURE 8 ATR-IR spectra of f-(xSx*A*/G)$_6$- (*dotted line*) and df-(xSx*A*/G)$_6$- (*solid line*) incorporated liposome preparations in D_2O showing a characteristic β-sheet-type hydrogen bond pattern with bands around 1627 and 1690 cm^{-1} (see Table 2 for % fraction of different secondary structures).

TABLE 2 Structural assignment from the ATR-IR spectra of peptide-incorporated liposome/D_2O preparations*

Peak positions, cm^{-1}	Peak area (%) f-(xSx*A*/G)$_6$	df-(xSx*A*/G)$_6$	f-(xSxG)$_6$	Structure assignment
1692	6.25	6.50	8.82	Antiparallel-β
1684	22.9	25.7	23.64	Antiparallel-β/turn
1669	5.30	4.57	7.93	Turn/loop
1652	5.10	5.80	6.57	α-Helix/disordered
1627	60.45	57.43	53.04	β-Sheet

*Fourier deconvolution of the amide 1 band followed by Gaussian fitting as the sum of five individual peaks. The percentage area of each component peak and structural assignment corresponding to the peak positions are shown. The possible errors are $\pm$5% for the peak areas and $\pm$2 cm^{-1} for the band positions. Deconvoluted spectra peak width 12 cm^{-1} and 45% smoothing used for Gaussian band fitting.

frequency band found in antiparallel β-sheet peptides due to transition dipole coupling is usually very weak compared to the low frequency band. So, one of the weaker components (1692 cm^{-1}) in the high frequency region (1660–1700 cm^{-1}) could be ascribed to the antiparallel hydrogen bonding and the rest to turn structures (24). A broad band around 1530 cm^{-1} in the amide 2 region (peptide-liposome samples in H_2O) further supported a β-structure (data not shown).

DISCUSSION

We noticed earlier that the ion channel properties of f-(xSxG)$_6$ and df-(xSxG)$_6$ peptides resemble those of β-barrel porin channels in several respects (9). The formation of highly conductive channels (mean single-channel conductance = 1.37 nS), the two state gating of the channels at potentials $>\pm$40 mV, the observation of fast and slow kinetic events, and the existence of subconductance states demonstrate such a similarity (9). The permeation of a wide variety of ions of different sizes suggests the formation of nonselective channels with a pore diameter >10.5 Å (corresponding to the calculated diameter of the largest permeating cation, NEt_3Bz^+). Based on these results we concluded that resemblance of (xSxG)$_6$ channels to that of porins could be due to the formation of a β-barrel-like structure possibly through peptide aggregation (9). This was further supported by CD and infrared (IR) studies indicating a β-sheet conformation in membranes stabilized by antiparallel hydrogen bonding and possibly some β-turns (9). Furthermore, inhibition of (xSxG)$_6$ channel by Congo red, oligomeric structures in association with lipid bilayers detected by electron microscopy, and gel electrophoresis of peptide-incorporated-liposomes indicating multimeric species suggests that (xSxG)$_6$ channels are formed by peptide aggregation (10).

In this work we hypothesized that an (LLLD)$_6$ pattern of sequence having a formyl group at the N-terminus would form a β^{12}-helical dimeric structure in membranes through hydrogen bonding between two β-helical monomers via

N-formyl groups as in gramicidin (11,17). Substantial variation in the ion channel properties of $(xSxG)_6$ upon D-alanine substitutions strongly suggests the formation of a different type of structural species in membranes. Here, we tried to validate the proposed β^{12}-helical model for f-$(xSxA/G)_6$ by combining several lines of independent structural and functional information. Most importantly, both the formyl and desformyl analogs of $(xSxG)_6$ were membrane active, whereas the desformyl analog of $(xSxA/G)_6$ did not form channels. Second, the formation of single channels without multiple states or subconductance states in the case of f-$(xSxA/G)_6$ suggests that the channels do not have a complex structure. Usually multiple conductance states of complex channels result from the cooperation of several individual pore-forming subunits or the presence of distinct conformational species of the same protein (25,26). Hence, these two possibilities can be eliminated in the case of the f-$(xSxA/G)_6$ channel. Moreover, low single-channel conductance (49.6 pS) and open channel events represented by a single time constant (τ) also rule out the possibility of a complex channel. So, the possibility of a channel formed from a single molecule or a dimer could be envisaged. Another interesting difference between the f-$(xSxG)_6$ and f-$(xSxA/G)_6$ channels is the absence of a voltage gating behavior in the latter. The fraction of open channels of f-$(xSxA/G)_6$ constitutes ~30–40% of total channel events over a wide range of applied potentials. The presence of distinct open and closing events might represent an equilibrium between conducting and nonconducting forms of the channel. Moreover, if a channel is formed from the f-$(xSxA/G)_6$ monomer one would expect that the channel would be open for a long period of time without several closing events and the fraction of open channel events would be high. However this assumption will be good only if no conformational changes of the peptide take place within the membrane. Based on the above discussion it is reasonable to believe that the f-$(xSxA/G)_6$ channel is formed by the association of two monomeric units via *N*-formyl groups. The effect of peptide concentration on channel conductance also supports the idea of a peptide dimer as the possible channel species. We could not observe current transitions by adding f-$(xSxA/G)_6$ just on one side of the membrane, suggesting that the f-$(xSxA/G)_6$ molecule cannot readily cross the membrane and the channel is probably formed by dimerization, one molecule approaching from each side of the bilayer. The possibility of a channel comprising α-helical or β-sheet structure is also ruled out based on the following considerations. First, the α-helical conformation would be less favored in the bilayer because serine side chains would be exposed to hydrocarbon tails in the interior of the membrane. Second, the pore formation by β- sheet peptides is known to proceed via aggregation, resulting in complex multichannels having several subconductance states (9,21,25,27).

The examination of the pore size of the f-$(xSxA/G)_6$ channel with a set of organic ammonium cations showed that the largest cation that is permeable through the channel is the ammonium cation, indicating that the diameter of the narrowest portion of the channel is ~4 Å (28). In the proposed β-helical model, the f-$(xSxA/G)_6$ channel comprises three peripheral pores each about the same internal diameter of the gramicidin channel (~4.5 Å). Or in other words, a β^{12}-helical structure is composed of three gramicidin-like pores. Space-filling molecular models showed that each pore has an internal diameter of ~4.5 Å. Though the maximum diameter of the β^{12} helix structure (from one end to other end of the β^{12}-helix) is expected to be three times that of gramicidin, the effective internal diameter for the passage of ions will be close to that of gramicidin as the channel interior is partly blocked by side chains of serine. This could explain the impermeability of membranes to larger cations such as NMe_4^+ and NEt_4^+. As explained earlier a salient feature of the proposed structure is that the serine hydroxyl groups lining the interior of the channel may solvate mobile ions, contributing to ion selectivity. The ionic selectivity of f-$(xSxA/G)_6$ channels ($pK^+/pCl^- = 6.9$) is consistent with the prediction that ions traversing the channel would be coordinated by serine hydroxyl groups. The hydroxyl group is an amphivalent ligand and may coordinate either anions or cations. The majority of the current is carried by cations because first, the oxygen atom of the OH dipole is more negative than the hydrogen atom is positive (thus the situation $HO–M^+–OH$ is more favorable, energetically, than $OH–X^-–HO$) and second, because geometric constraints within the channel would not allow a favorable $OH–X^-$ bond when the anion is in one of the three peripheral pores of the channel. In addition, the walls of the channel are composed of peptide groups which can supply a part of the coordination sphere for the ions in transit, and the same argument about the relative strengths of the oxygen and hydrogen atom in the peptide group applies (29). For these reasons cations would be accommodated much more readily than anions in the three peripheral chambers of the channel.

Even though conformational studies using IR and CD spectral methods cannot ascertain the exact structure of a peptide in membranes, they can give valuable clues regarding the nature of hydrogen bonding and backbone structure. Distinct spectral features of f-$(xSxA/G)_6$ in membranes compared to that of f-$(xSxG)_6$ suggest a structural change upon incorporating D-alanines instead of glycine residues. The CD spectrum of f-$(xSxG)_6$ had the characteristic feature of a β-sheet protein with a maximum and minimum around 205 and 220 nm, respectively, in membranes (22,30). However, the CD spectrum of f-$(xSxA/G)_6$ is different from that of typical β-sheet proteins in having an additional negative band around 226 nm along with negative and positive bands around 215 and 200 nm, respectively. The presence of two minima is usually ascribed to α-helical structures but at different positions (209 and 222 nm) than in f-$(xSxA/G)_6$ peptide (30). Moreover, the IR study did not show any evidence of an α-helical structure in membranes and indicated a β-sheet-type hydrogen-bonding pattern (31). Considering

the influence of one tryptophan residue present in f-(xSx*A*/G)$_6$, the 226 nm band could also arise from changes in the tryptophan environment. For example, membrane-bound tryptophan-containing short peptides are reported to show a similar peak around 230 nm (1,32). A comparison of the CD spectra of f-(xSx*A*/G)$_6$ in membrane and methanol solution seems to support the idea of an environment-sensitive dichroism of tryptophan residue due to the absence of a 226 nm band in the latter. However, the absence of a similar band in the spectrum of f-(xSxG)$_6$ (which also has one tryptophan) in a membrane environment suggests that the 226 nm band arises more likely from a change in backbone conformation of the f-(xSx*A*/G)$_6$ peptide and subsequent variation in the microenvironment of tryptophan residue upon D-alanine substitution. Taken together, the data indicate that f-(xSx*A*/G)$_6$ has a different backbone structure compared to α-helical and β-sheet proteins and is stabilized by β-sheet-type hydrogen bonding.

A comparison of conductance values of f-(xSx*A*/G)$_6$ in this study and that of gA reported in the literature revealed that, interestingly, both peptides have almost the same single-channel conductance in DPhPC lipid bilayers (49.6 pS for f-(xSx*A*/G)$_6$ and 47.2 for gA) in the presence of 1 M CsCl (33). However, it is known that the conductance of the gA channel arises in part from the presence of four tryptophan residues which alter the energy profile for ion permeation through long-range electrostatic interactions (34). For example, an ~5-fold decrease in single-channel conductance of gA was observed upon substituting three tryptophan residues with phenylalanines (35). So it would be more appropriate to compare the single-channel conductance of f-(xSx*A*/G)$_6$ (has only one tryptophan) with that of a gramicidin analog having only one tryptophan residue; an ~9-fold difference in the single-channel conductance of f-(xSx*A*/G)$_6$ (30 pS in 1 M NaCl) compared to the gA analog (3.4 pS in 1 M NaCl) having one tryptophan residue (35) implies that the presence of three peripheral pores with an overall diameter three times that of the gramicidin channel and the presence of serine hydroxyl groups which can coordinate permeating ions may be contributing to the higher conductivity of f-(xSx*A*/G)$_6$ channel.

In summary, this work demonstrates a dramatic change in ion channel and conformational properties of a (xSxG)$_6$ peptide upon replacing glycine residues with D-alanines. Significant changes in the structural and functional properties as a result of glycine to D-alanine substitution of (xSxG)$_6$ suggest that D-amino acid recurrence in a peptide sequence overwhelmingly affect the backbone structure of the peptide in membranes. Moreover, glycines in (xSxG)$_6$ seem to have a structural role in aggregation and in the formation of β-barrel-like pore formation due to their flexibility, lack of side chains, and the ability to facilitate sheet-to-sheet packing interactions. Using a simple β^{12}-helical model, we proposed that the ion channel properties of D-alanine repeat (f-(xSx*A*/G)$_6$) peptide could be easily explained and correlated with the structure. We hope that the success in correlating the functional properties of the channel with the proposed β-helical model will stimulate the design of gramicidin-like β-helical motifs with a variety of applications. Moreover, the transformation of a complex porin-like channel into a simple gramicidin-like channel through glycine to D-alanine substitutions provides an interesting possibility for the structural engineering of different pore-forming β-sheet proteins in the design of novel macromolecular devices. With the ability to predict structural models of smaller proteins and to correlate with their functional properties, we are moving toward the ultimate goal of understanding the dependence of protein sequence on conformation, folding, and function.

We thank Cary Pritchard, Dept. of Chemistry, Indiana University-Purdue University Indianapolis, Indianapolis, IN, for his technical assistance with CD and ATR-IR spectroscopic analysis, and Zhidong Zhang for helping in the mass spectroscopic analysis.

REFERENCES

1. Wimley, W. C., K. Hristova, A. S. Ladokhin, L. Silvestro, P. H. Axelsen, and S. H. White. 1998. Folding of β-sheet membrane proteins: a hydrophobic hexapeptide model. *J. Mol. Biol.* 277:1091–1110.
2. Bishop, C. M., W. F. Walkenhorst, and W. C. Wimley. 2001. Folding of β-sheets in membranes: specificity and promiscuity in peptide model systems. *J. Mol. Biol.* 309:975–988.
3. Rausch, J. M., J. R. Marks, and W. C. Wimley. 2005. Rational combinatorial design of pore-forming β-sheet peptides. *Proc. Natl. Acad. Sci. USA.* 102:10511–10515.
4. Trzesniewska, K., M. Brzyska, and D. Elbaum. 2004. Neurodegenerative aspects of protein aggregation. *Acta Neurobiol. Exp. (Warsz.).* 64:41–52.
5. Arispe, N. 2004. Architecture of the Alzheimers AβP ion channel pore. *J. Membr. Biol.* 197:33–48.
6. Lin, H., R. Bhatia, and R. Lal. 2001. Amyloid β protein forms ion channels: implications for Alzheimer's disease pathophysiology. *FASEB J.* 15:2433–2444.
7. Quist, A., I. Doudevski, R. Azimova, D. Ng, B. Frangione, B. Kagan, J. Ghiso, and R. Lal. 2005. Amyloid ion channels: a common structural link for protein-misfolding disease. *Proc. Natl. Acad. Sci. USA.* 102: 10427–10432.
8. Wimley, W. C. 2003. The versatile β-barrel membrane protein. *Curr. Opin. Struct. Biol.* 13:404–411.
9. Thundimadathil, J., R. W. Roeske, and L. Guo. 2005. A synthetic peptide forms voltage-gated porin-like ion channels in lipid bilayer membranes. *Biochem. Biophys. Res. Commun.* 330:585–590.
10. Thundimadathil, J., R. W. Roeske, H.-Y. Jiang, and L. Guo. 2005. Aggregation and porin-like channel activity of a β-sheet peptide. *Biochemistry.* 44:10259–10270.
11. Ketchem, R. R., W. Hu, and T. A. Cross. 1993. High-resolution conformation of gramicidin A in a lipid bilayer by solid-state NMR. *Science.* 261:1457–1460.
12. Townsley, L. E., W. A. Tucker, S. Sham, and J. F. Hinton. 2001. Structures of gramicidins A, B, and C incorporated into sodium dodecyl sulfate micelles. *Biochemistry.* 40:11676–11686.
13. Navarro, E., R. Tejero, E. Fenude, and B. Celda. 2001. Solution NMR structure of a D, L alternating oligonorleucine as a model of β helix. *Biopolymers.* 59:110–119.
14. Sanchez-Quesada, J., H. S. Kim, and M. R. Ghadiri. 2001. A synthetic pore-mediated transmembrane transport of glutamic acid. *Angew. Chem. Int. Ed. Engl.* 40:2503–2506.

15. Cornelissen, J. J. L. M., J. J. J. M. Donnoers, R. D. Helder, W. S. Graswinckel, G. A. Metselaar, A. E. Rowan, N. A. J. M. Sommerdijk, and R. J. M. Nolte. 2001. β-helical polymers from isocyanopeptides. *Science*. 293:676–678.

16. Kennedy, S. J., H. R. Besch, A. M. Watanabe, A. R. Freeman, and R. W. Roeske. 1977. Properties of beta-helical ion channels. *Biophys. J*. 17:A87–A87. (Abstr.)

17. Kennedy, S. J. 1978. Structures of membrane proteins. *J. Membr. Biol*. 42:265–279.

18. Benz, R., K. Janko, W. Boos, and P. Lauger. 1978. Formation of large, ion-permeable membrane channels by the matrix protein (porin) of Escherichia coli. *Biochim. Biophys. Acta*. 511:305–319.

19. Wallace, B. A., and E. R. Blout. 1979. Conformation of an oligopeptide in phospholipid vesicles. *Proc. Natl. Acad. Sci. USA*. 76: 1775–1779.

20. Hille, B. 1992. Ion Channels of Excitable Membranes. Sinauer, Sunderland, MA.

21. Lin, M.-C. A., and B. L. Kagan. 2002. Electrophysiological properties of channels induced by Aβ25–35 in planar lipid bilayers. *Peptides*. 23:1215–1228.

22. Johnson, W. C. Jr. 1988. Secondary structure of proteins through circular-dichroism spectroscopy. *Annu. Rev. Biophys. Biophys. Chem*. 17:145–166.

23. Chirgadze, Y. N., O. V. Fedorov, and N. P. Trushima. 1975. Estimation of amino acid residue side chain absorption in the infrared spectra of protein solutions in heavy water. *Biopolymers*. 14:679–694.

24. Barth, A., and C. Zscherp. 2002. What vibrations tell us about proteins. *Q. Rev. Biophys*. 35:369–430.

25. Hirakura, Y., M.-C. Lin, and B. L. Kagan. 1999. Alzheimer amyloid Aβ 1–42 channels: effects of solvent, pH, and Congo red. *J. Neurosci. Res*. 57:458–466.

26. Minn, A. J., P. Velez, S. L. Schendel, H. Liang, S. W. Muchmore, S. W. Fesik, M. Fill, and C. B. Thompson. 1997. Bcl-XL forms an ion channel in synthetic lipid membranes. *Nature*. 385:353–357.

27. Tobkes, N., B. A. Wallace, and H. Bayley. 1985. Secondary structure and assembly mechanism of an oligomeric channel protein. *Biochemistry*. 24:1915–1920.

28. Qi, Z., M. Sokabe, K. Donowaki, and H. Ishida. 1999. Structure-function study on a de novo synthetic hydrophobic ion channel. *Biophys. J*. 76:631–641.

29. Koeppe II, R. E., J.-L. Mazet, and O. S. Andersen. 1990. Distinction between dipolar and inductive effects in modulating the conductance of gramicidin channels. *Biochemistry*. 29:512–520.

30. Sreerama, N., and R. W. Woody. 2004. Computation and analysis of protein circular dichroism spectra. *Methods Enzymol*. 383:318–351.

31. Krimm, S., and J. Bandekar. 1986. Vibrational spectroscopy and conformation of peptides, polypeptides and proteins. *Adv. Protein Chem*. 38:181–364.

32. Ladokhin, A. S., M. E. Selsted, and S. H. White. 1997. Bilayer interactions of indolicidin, a small antimicrobial peptide rich in tryptophan, proline, and basic amino acids. *Biophys. J*. 72:794–805.

33. Mattice, G. L., and R. E. Koeppe II. 1995. Stabilizing effect of D-alanine in gramicidin channels. *Biochemistry*. 34:6827–6837.

34. Fonseca, V., P. Daumas, L. Ranjalahy-Rasoloarijao, F. Heitz, R. Lazaro, Y. Trudelle, and O. S. Andersen. 1992. Gramicidin channels that have no tryptophan residues. *Biochemistry*. 31:5340–5350.

35. Becker, M. D., D. V. Greathouse, R. E. Koeppe II, and O. S. Andersen. 1991. Amino acid sequence modulation of gramicidin channel function. Effects of tryptophan-to-phenylalanine substitutions on the single channel conductance and duration. *Biochemistry*. 30:8830–8839.